Magnetic structure and dispersion relation of the $S = \frac{1}{2}$ quasi-one-dimensional Ising-like antiferromagnet $BaCo_2V_2O_8$ in a transverse magnetic field

M. Matsuda,[1] H. Onishi,[2] A. Okutani,[3] J. Ma,[1,*] H. Agrawal,[4] T. Hong,[1] D. M. Pajerowski,[5,†]
J. R. D. Copley,[5] K. Okunishi,[6] M. Mori,[2] S. Kimura,[7] and M. Hagiwara[3]

[1]*Quantum Condensed Matter Division, Oak Ridge National Laboratory, Oak Ridge, Tennessee 37831, USA*
[2]*Advanced Science Research Center, Japan Atomic Energy Agency, Tokai, Ibaraki 319-1195, Japan*
[3]*Center for Advanced High Magnetic Field Science, Graduate School of Science, Osaka University, Osaka 560-0043, Japan*
[4]*Instrument and Source Division, Oak Ridge National Laboratory, Oak Ridge, Tennessee 37831, USA*
[5]*NIST Center for Neutron Research, Gaithersburg, Maryland 20899-6102, USA*
[6]*Department of Physics, Niigata University, Niigata 950-2181, Japan*
[7]*Institute for Materials Research, Tohoku University, Sendai 980-8577, Japan*

(Received 16 May 2017; published 25 July 2017)

$BaCo_2V_2O_8$ consists of Co chains in which a Co^{2+} ion carries a fictitious spin $\frac{1}{2}$ with Ising anisotropy. We performed elastic and inelastic neutron scattering experiments in $BaCo_2V_2O_8$ in a magnetic field perpendicular to the c axis which is the chain direction. With applying magnetic field along the a axis at 3.5 K, the antiferromagnetic order with the easy axis along the c axis, observed in zero magnetic field, is completely suppressed at 8 T, while the magnetic field gradually induces an antiferromagnetic order with the spin component along the b axis. We also studied magnetic excitations as a function of transverse magnetic field. The lower boundary of the spinon excitations splits gradually with increasing magnetic field. The overall feature of the magnetic excitation spectra in the magnetic field is reproduced by the theoretical calculation based on the spin $\frac{1}{2}$ XXZ antiferromagnetic chain model, which predicts that the dynamic magnetic structure factor of the spin component along the chain direction is enhanced and that along the field direction has clear incommensurate correlations.

DOI: 10.1103/PhysRevB.96.024439

I. INTRODUCTION

One-dimensional (1D) Heisenberg antiferromagnet, carrying spin (S) $\frac{1}{2}$, has been studied intensively, because it exhibits exotic phenomena originating from the quantum effect [1]. The $S = \frac{1}{2}$ 1D antiferromagnet with Ising-like anisotropy also shows an interesting quantum effect in the presence of an external magnetic field along the chain, which drives the long range ordered phase to a spin-liquid phase. This is due to the incommensurate spin correlation in the quantum critical state, developed in the longitudinal magnetic field [2,3]. The finite interchain interactions give rise to a long range longitudinal spin-wave-density (SDW) phase and the incommensurability changes with magnetic field.

It was found that $BaCo_2V_2O_8$ shows such an interesting phenomenon in longitudinal magnetic field [4–6]. $BaCo_2V_2O_8$ consists of screw-type chains of Co^{2+} along the c axis, as shown in Fig. 1(a), in which Co^{2+} ions carry fictitious spin $\frac{1}{2}$. This material shows an antiferromagnetic (AF) structure with the easy axis along the c axis and the magnetic wave vector of $\mathbf{k_f} = (0,0,1)$ below $T_N = 5.4$ K in zero magnetic field. The magnetic arrangement is antiferromagnetic along the screw-type chain (the c axis) and ferromagnetic and antiferromagnetic along the a and b axis, respectively [7]. The magnetic order is gradually suppressed in magnetic field along the chain direction. A long-range SDW phase is induced by an external longitudinal magnetic field of ∼4 T along the spin direction below ∼1.7 K [4,6,8–10].

Interestingly, transverse magnetic field was also found to affect the magnetic order at relatively low magnetic fields in $BaCo_2V_2O_8$ [8,10], although canted antiferromagnetic state is stable up to high magnetic fields in the usual $S = \frac{1}{2}$ XXZ spin chain [11]. In particular, when the magnetic field is applied along the a axis, the magnetic order at zero magnetic field is suppressed at ∼10 T. Kimura *et al.* showed that the effective field induced perpendicular to the external field can suppress the long-range magnetic order [8]. The effective field is considered to be induced by the screw chain structure, where the apical Co-O bond of the CoO_6 octahedron is tilted by 4.8° from the c axis. There are four distorted CoO_6 octahedra in a unit cell along the c axis and the directions of the magnetic principal axes of the four apical Co-O bonds are different. Therefore, the effective fields have four-step periodicity. Due to the tilting of the magnetic principle axes, the g tensor has off-diagonal elements in the Cartesian coordinate system of the crystal axes, which generates the effective fields perpendicular to the external field. According to the $S = \frac{1}{2}$ XXZ AF chain model with the effective local fields included, in the case of the external field along the a axis, the transverse fields induced along the b and c axes are "up-down-up-down" and "up-up-down-down" type, respectively, as shown in Fig. 1(b). This model reproduces the magnetization data well [8]. However, there has been no direct experimental evidence to confirm the effective fields.

The quantum spin chain system is also known to show exotic magnetic excitations, e.g., the spinon excitation. The magnetic field effect on the spinon excitations in $S = \frac{1}{2}$ 1D Heisenberg AF chain was studied theoretically in detail

*Present address: Department of Physics and Astronomy, Shanghai Jiao Tong University, Shanghai 200240, People's Republic of China.
†Present address: Quantum Condensed Matter Division, Oak Ridge National Laboratory, Oak Ridge, Tennessee 37831, USA.

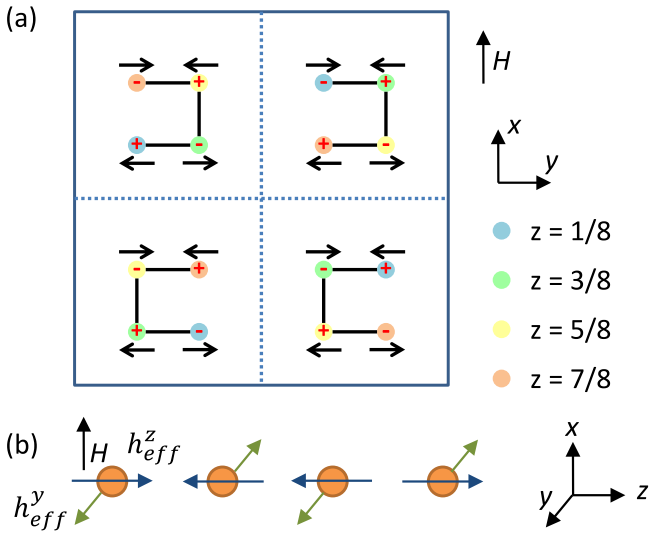

FIG. 1. (a) Co^{2+} ions in a unit cell projected onto the *ab* plane. "+" and "−" represent the spin directions along the *c* axis in zero field. Horizontal arrows represent the staggered magnetic field induced perpendicular to the magnetic field. (b) A schematic view of the simplified Co chain in $BaCo_2V_2O_8$. *X* and *Z* are defined along the magnetic field and chain directions, respectively. *Y* is perpendicular to both *X* and *Z*. When the magnetic field is applied along *X*, effective magnetic fields with $+-+-$ ($h^Y_{\rm eff}$) and $+--+$ ($h^Z_{\rm eff}$) are induced along *Y* and *Z*, respectively.

[12–15]. Coldea *et al.*, Dender *et al.*, and Stone *et al.* observed excitation modes in Cs_2CuCl_4 [16], $Cu(C_6D_5COO)_2 \cdot 3D_2O$ [17], and $Cu(C_4D_4N_2)(NO_3)_2$ [18], respectively, under magnetic fields, which are not explained by the linear spin-wave theory but by the theories based on the quantum spin model [12–15]. It is interesting to study the magnetic field dependence of the magnetic excitations in the quantum Ising-like system as well as the effect of staggered field on the excitation spectra.

We performed elastic and inelastic neutron scattering experiments in $BaCo_2V_2O_8$ in a magnetic field along the *a* axis. We observed that the Néel order at zero magnetic field, which has a spin component along the *c* axis, is suppressed with increasing field and completely suppressed at 8 T at 3.5 K. We also found that the AF order with a spin component along the *b* axis gradually develops with increasing field. This is the direct observation of the induced effective field along the *b* axis with up-down-up-down. Furthermore, the magnetic field dependence of the spinon excitations was studied. Although the uniform magnetic field effect was studied previously, the staggered field effect has not been investigated. The comparison between the theoretical calculations based on the $S = \frac{1}{2}$ *XXZ* AF chain model with and without staggered field clarified the effect of staggered magnetic field. This effect appears as a strong dynamic magnetic structure factor of the spin component along the field direction and clear incommensurate correlations of the spin component along the field direction. These features are in good agreement with experimental results.

II. EXPERIMENTAL METHOD

Single crystals of $BaCo_2V_2O_8$ were grown by the traveling solvent floating zone (TSFZ) method in air. The inelastic neutron scattering experiments were carried out on a disk chopper spectrometer (DCS) [19] installed at the NIST Center for Neutron Research (NCNR) and a cold neutron triple-axis spectrometer (CTAX) installed at the High Flux Isotope Reactor (HFIR) at Oak Ridge National Laboratory (ORNL). The dimensions of the rod shaped crystals used on DCS and CTAX are $\sim 6\Phi \times 40$ and $\sim 6\Phi \times 20$ mm^3, respectively. We utilized incident energies of 13.1 meV on DCS. Energy resolution at the elastic position is ∼0.8 meV. Neutrons with a final energy of 5 meV were used, together with a horizontal collimator sequence of guide–open–S–80′–open on CTAX. Energy resolutions at the elastic position is ∼0.25 meV. Contamination from higher-order beams was effectively eliminated using a cooled Be filter. On both instruments, the single crystals were oriented in the $(0kl)$ scattering plane and were mounted in vertical field cryomagnets. The magnetic field is applied along the *a* axis. The analysis and visualization of the DCS data were performed using a software DAVE [20].

III. THEORETICAL MODEL AND METHOD

The AF chain in $BaCo_2V_2O_8$ is well described by the $S = \frac{1}{2}$ *XXZ* AF chain model [8], which gives the following Hamiltonian:

$$H = J \sum_j \{S_{j,z}S_{j+1,z} + \epsilon(S_{j,x}S_{j+1,x} + S_{j,y}S_{j+1,y})\} - \mu_B \sum_j \mathbf{S}_j \tilde{g} \mathbf{H_0}, \quad (1)$$

where J, ϵ, μ_B, $\tilde{g}$, and $\mathbf{H_0}$ are the nearest-neighbor exchange interaction, the ratio between anisotropic exchange interactions parallel and perpendicular to the easy axis, the Bohr magneton, a g tensor, and the external magnetic field, respectively.

As described in Sec. I, the magnetic chain of the Co^{2+} ions in $BaCo_2V_2O_8$ is the screw type with distorted CoO_6 octahedra, which has four step periodicity. Due to the tilting of the magnetic principle axes, the g tensor has off-diagonal elements in the Cartesian coordinate system of the crystal axes, which generates the effective fields perpendicular to the external field. Therefore, the effective Hamiltonian can be described as

$$H = J \sum_j \{S_{j,Z}S_{j+1,Z} + \epsilon(S_{j,X}S_{j+1,X} + S_{j,Y}S_{j+1,Y})\} - \mu_B \sum_j \left\{ g_{XX} H_0 S_{j,X} + h_Y S_{j,Y} \sin[2\phi_1 + \pi(j-1)] + h_Z S_{j,Z} \cos\left[\phi_1 + \frac{\pi(j-1)}{2}\right] \right\}. \quad (2)$$

Here *X* and *Z* correspond to the magnetic field direction ($\parallel a$ axis) and the chain direction ($\parallel c$ axis), respectively. *Y* ($\parallel b$ axis) is perpendicular to both *X* and *Z*. h_Y and h_Z are the absolute value of the effective field for the *Y* and *Z* direction.

ϕ_1 is the angle between Y and a magnetic principal axis and is set at $\pi/4$ in this study.

In order to clarify magnetic excitations of the effective model (2), we calculated dynamical spin structure factors along $\mathbf{Q} = (0,0,Q)$ at zero temperature, defined by

$$S(Q,E)^{\alpha\alpha} = -\frac{1}{\pi}\mathrm{Im}\langle\psi_{\mathrm{G}}|S^{\dagger}_{Q,\alpha}\frac{1}{E+E_{\mathrm{G}}-H+i\eta}S_{Q,\alpha}|\psi_{\mathrm{G}}\rangle, \tag{3}$$

where $S_{Q,\alpha}$ is the Fourier transform of the α component of the spin operator, $|\psi_{\mathrm{G}}\rangle$ is the ground state, and E_{G} is the ground-state energy. An infinitesimal value η is set to 0.1 in units of J. To obtain the magnetic excitation spectra, we used density-matrix renormalization group (DMRG) techniques with open boundary conditions [21,22]. Note that the total magnetization is not conserved because of transverse magnetic fields, so that we cannot utilize the total magnetization to reduce the size of the Hilbert space.

Here we note that magnetic moments are induced by magnetic fields, leading to a Lorentzian peak of width η at zero energy. Such a Lorentzian peak also appears in $S(Q=\pi,E)^{ZZ}$ for the Néel phase originating from the Ising-like anisotropy at low magnetic fields. As the field-induced magnetic moments increase, the corresponding Lorentzian peak grows and masks excitation spectra at finite energy. To subtract the contribution of the finite magnetic moments to the spectral intensity, it is useful to measure dynamical structure factors of spin fluctuations $\tilde{S}_{j,\alpha} = S_{j,\alpha} - \langle S_{j,\alpha}\rangle$, given by

$$\begin{aligned}\tilde{S}(Q,E)^{\alpha\alpha} &= -\frac{1}{\pi}\mathrm{Im}\langle\psi_{\mathrm{G}}|\tilde{S}^{\dagger}_{Q,\alpha}\frac{1}{E+E_{\mathrm{G}}-H+i\eta}\tilde{S}_{Q,\alpha}|\psi_{\mathrm{G}}\rangle \\ &= S(Q,E)^{\alpha\alpha} - \frac{1}{\pi}\frac{\eta}{E^2+\eta^2}\langle S_{Q,\alpha}\rangle^2,\end{aligned} \tag{4}$$

where the second term represents the Lorentzian peak at zero energy originating from the magnetic moments. We will present results of $\tilde{S}(Q,E)^{\alpha\alpha}$ in Sec. IV B.

We performed DMRG calculations with 64 sites, using the parameters in Ref. [8], i.e., $J = 65$ K, $\epsilon = 0.46$, $g_{XX} = 2.75$, $h_Y/g_{XX}H_0 = 0.4$, and $h_Z/g_{XX}H_0 = 0.1 \times \sqrt{2}$, which were evaluated to explain the magnetization curve. We did not perform refinement of parameters, but concentrated our effort on the clarification of overall features of the magnetic excitation spectra of the effective model (2). The number of states kept in renormalization steps is 40, and the truncation error is typically 10^{-4}–10^{-5}. The system size and the kept states are sufficiently large to obtain converged numerical data.

IV. RESULTS AND DISCUSSION

A. Magnetic structure in transverse field

Magnetic Bragg peaks develop at (h,k,l) with $h+k+l =$ odd, i.e., (0, odd, even) and (0, even, odd) in the $(0kl)$ plane, below $T_{\mathrm{N}} = 5.4$ K. Figure 2(a) shows magnetic field dependence of the magnetic Bragg intensities. (0, 2, 1) and (0, 4, 1) intensities slightly increase with increasing magnetic field up to 5 T, then start to decrease and become completely suppressed at 8 T. Large hysteresis was reported in Ref. [10], which is interpreted to be due to magnetic domain effect. We also observed such a hysteresis behavior in Fig. 2(a),

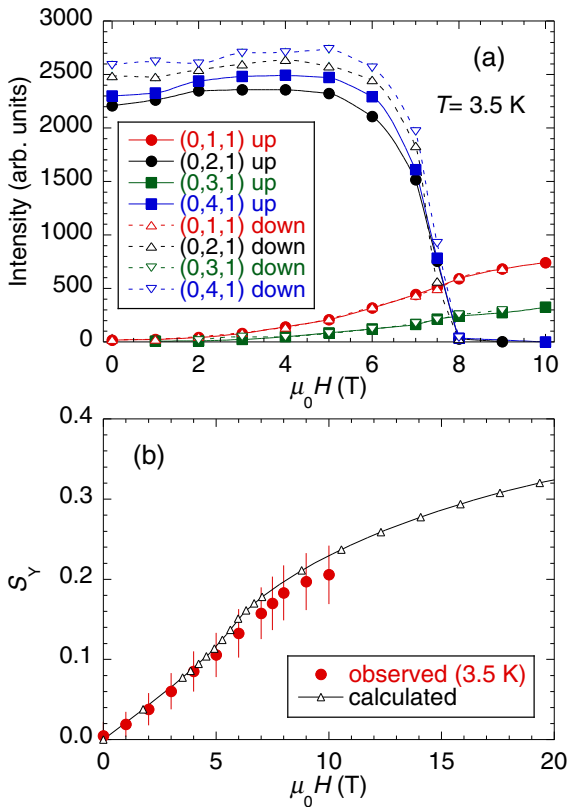

FIG. 2. (a) Magnetic Bragg peak intensities as a function of magnetic field measured at 3.5 K on CTAX. Filled and open symbols represent intensities measured while ramping up and down the magnetic field, respectively. (b) Observed and calculated staggered magnetic moment along the b axis as a function of magnetic field.

but the difference of the intensities between ramping up and down processes is much smaller than that in Ref. [10], which reported that the intensities are different by a factor of 2. The difference of the hysteresis behavior probably originates from the sample temperature, 3.5 K and 50 mK in the present study and Ref. [10], respectively. It is reasonable that the hysteresis becomes more enhanced at lower temperatures.

It is found that new magnetic Bragg peaks appear at (0, odd, odd) in the magnetic field. (0, 1, 1) and (0, 3, 1) intensities gradually increase with increasing magnetic field, as shown in Fig. 2(a). We found that the magnetic structure factors calculated with the AF structure model, assuming that the magnetic moments are induced by the staggered fields in Fig. 1(a), reproduce the positions and relative intensities of the magnetic Bragg peaks. The magnetic moment of the ordered component along the b axis is calculated by comparing to nuclear Bragg intensities of (0, 2, 0) and (0, 2, 2). The magnetic field dependence of the ordered moment is plotted in Fig. 2(b). In order to convert from observed value $g_{YY}S_Y$ to S_Y, where g_{YY} and S_Y are the diagonal component of the g factor matrix along Y direction and spin value, along Y direction, respectively, we used the g_{YY} value of 2.75 which is reported in Ref. [8]. The calculated moment as a function of magnetic field, obtained using parameters in Ref. [8], reproduces the observed one reasonably well. This result indicates that this

AF order is driven by the staggered magnetic field induced perpendicular to the external field direction.

It is reported in Ref. [8] that the magnetic moments along the c axis (S_Z) with an arrangement of up-up-down-down along the c axis is predicted to appear above the critical field. We searched for the induced magnetic order at 10 T above the critical field at 3.5 K. However, no magnetic signal related to the c axis spin component was observed. S_Z predicted theoretically at 10 T is $\sim 0.04\mu_B$, which would be too small to be detected.

Here we summarize the magnetic field dependence of each spin component. S_X along the magnetic field direction is the moment induced ferromagnetically, which gradually develops with increasing field. Theoretical calculation predicts that the moment is $\sim 0.05\mu_B$ at 10 T. The magnetic intensity should be superposed on the nuclear Bragg peaks, but the intensity is expected to be too weak to be detected in our measurements. S_Y shows "up-down-up-down" type static order along the c axis induced by the staggered field with $S_Y \sim 0.2$ at 8 T, which is consistent with the theoretical prediction, as shown in Fig. 2(b). S_Z loses up-down-up-down type static order along the c axis at 8 T and 3.5 K. It is theoretically predicted that "up-up-down-down" type magnetic field destroys the magnetic order and the magnetic order with up-up-down-down develops along the c axis gradually above the critical field. The theoretically predicted moment is as small as $\sim 0.04\mu_B$ at 10 T, which is too small to be detected.

B. Magnetic excitations in transverse field

1. Experimental results

As described in Sec. III A, it is found that the effective local field is induced perpendicular to the external magnetic field along the a axis. We have studied the magnetic excitations in transverse magnetic field and also in the effective magnetic field perpendicular to it. Figure 3 shows energy cuts of the inelastic neutron scattering intensity in the $(0kl)$ plane measured at 3.5 K. The spectra are integrated over the energy range of $1.5 \leqslant E \leqslant 2.5$ meV. The scatterings elongated along k are observed around (0, 3, 1), (0, 0, 2), and (0, 6, 2) at zero magnetic field. In the simple chain system, the scattering intensity perpendicular to the chain direction only depends on the magnetic form factor. In $BaCo_2V_2O_8$, the dynamic magnetic structure factor modulates perpendicular to the chain direction because of the screw-type chain structure. Since there are four chains in a unit cell, as shown in Fig. 1(a), there should be four excitation modes. Two modes are degenerate so that the two different modes can be observed. In one mode, lower edge of the spinon excitation has minima and maxima at l = even and odd, respectively. In another mode, the minima and maxima positions are reversed. At 10 T, the excitations split along l direction. As will be shown below, the magnetic field decreases the gap energy for the S_Z excitations and change the spinon excitations from being commensurate to incommensurate along the chain for the S_X excitations. Both effects split the excitations along l direction.

Figures 4(a)–4(f) show the magnetic field dependence of the magnetic excitation spectra along l direction measured at 3.5 K. As described above, there are two magnetic excitation modes. We chose a mode with the magnetic zone center at

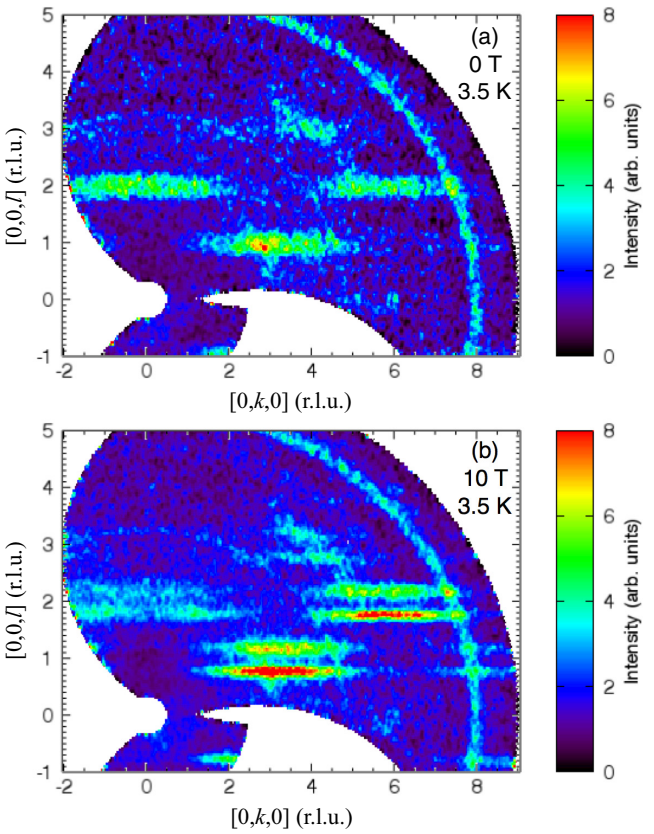

FIG. 3. Energy cuts of the inelastic neutron scattering intensity at 0 T (a) and 10 T (b) in the $(0kl)$ plane measured at $T = 3.5$ K with $E_i = 13.1$ meV on DCS. The scattering intensity is integrated in an energy range of $1.5 \leqslant E \leqslant 2.5$ meV. The arc-shaped scatterings are background signal from the aluminum sample holder.

l = even. In order to exclude another mode, we avoided to use data in the range of $1 < k < 5$. However, there is still a small contribution from the other mode stemming from l = odd. It is noted that due to the neutron polarization factor, the scattering intensities observed at (0, 0, 2), shown in Figs. 4(a), 4(c) and 4(e), originate from 100% of S_X and S_Y components. At (0, 6, 2), shown in Figs. 4(b), 4(d) and 4(f), 100%, 20%, and 80% of S_X, S_Y, and S_Z components are observed, respectively. The magnetic signal is stronger at a smaller l value due to the magnetic form factor.

At zero magnetic field, spinon excitations, typical magnetic excitations from the quantum Heisenberg AF chain, were observed, as shown in Figs. 4(a) and 4(b). The small gap of 1.8 meV comes from the Ising-like anisotropy. We calculated the dispersion using the exact diagonalization method. The dispersion can be well explained by the calculated value with $J = 6.25$ meV and $\epsilon = 0.44$. These values are consistent with $J = 5.6$ meV and $\epsilon = 0.46$, evaluated to explain the magnetization curve for $H \parallel c$ [8] and $J = 4.8$ meV and $\epsilon = 0.56$ from an inelastic neutron scattering experiment [23].

With increasing magnetic field along the a axis, the dispersion changes gradually. In particular, the low energy excitations below $\sim$4 meV around the magnetic zone center looks differently at (0, 0, 2) and (0, 6, 2). In order to observe the low energy magnetic excitations more clearly, we

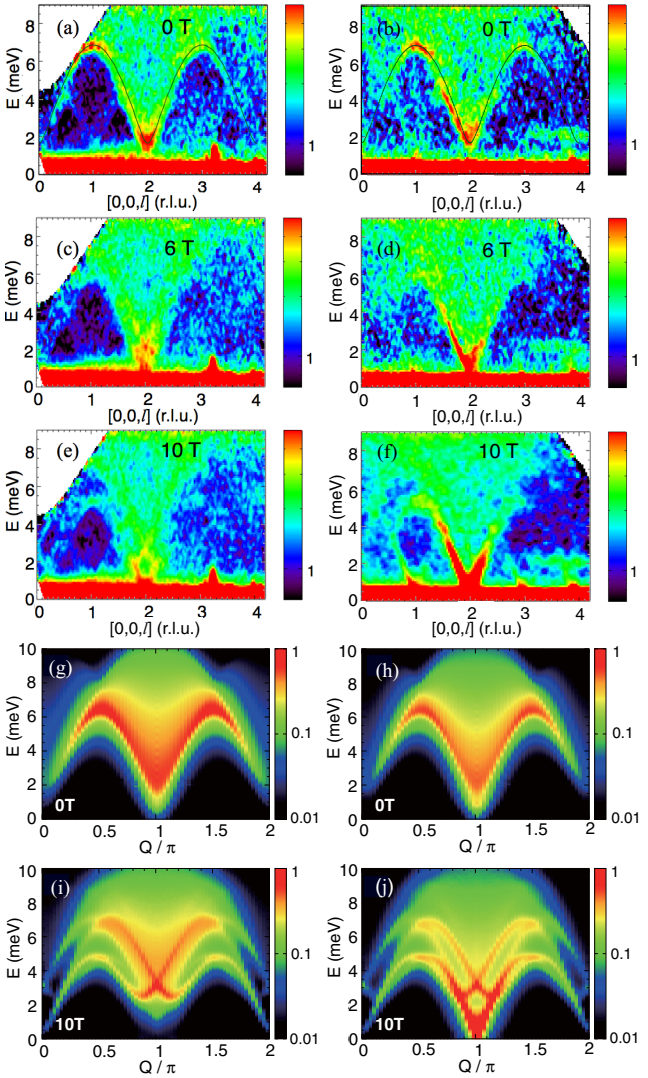

FIG. 4. (a)–(f) Contour maps of the inelastic neutron scattering intensity $S(Q,E)$ for $BaCo_2V_2O_8$ single crystal measured at $\mu_0 H =$ 0, 6, and 10 T and $T = 3.5$ K with $E_i = 13.1$ meV on DCS. The energy resolution is 0.8 meV at the elastic position. The spectra of (a), (c), and (e) and (b), (d), and (f) are integrated in the range of $-1 \leqslant k \leqslant 1$ and $5 \leqslant k \leqslant 6.5$, respectively. The intensity is shown in logarithmic scale. The solid curves in (a) and (b) are the lower boundary of the spinon excitations calculated for the $S = \frac{1}{2}$ XXZ AF chain model with $J = 6.25$ meV and $\epsilon = 0.44$. $l = 0$, 2, and 4 correspond to $Q = 0$, π, and 2π, respectively. (g)–(j) $\tilde{S}(Q,E)$ calculated by the DMRG method using the spin Hamiltonian [Eq. (2)]. To directly compare with the experimental data, appropriate fractions of spin components are summed up: 100% of S_X and S_Y components for (0,0,2) [(g) and (i)]; 100%, 20%, and 80% of S_X, S_Y, and S_Z components, respectively, for (0,6,2) [(h) and (j)]. (g) and (h) and (i) and (j) are for 0 and 10 T, respectively.

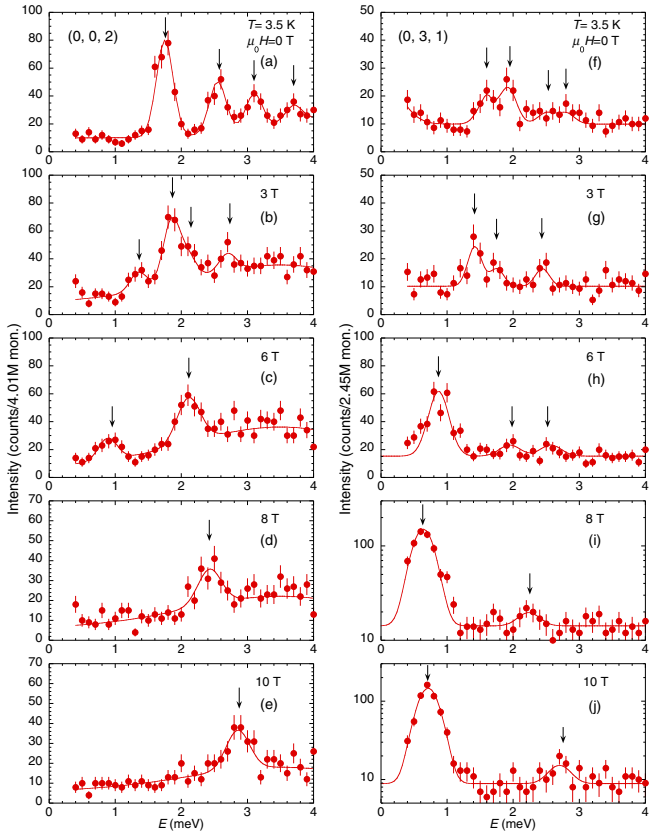

FIG. 5. Magnetic excitation spectra as a function of magnetic field measured at $T = 3.5$ K with $E_f = 5$ meV on CTAX. The energy resolution is 0.25 meV at the elastic position. The spectra of (a)–(e) and (f)–(j) were measured at (0, 0, 2) and (0, 3, 1), respectively. The arrows indicate the excitation peak positions. The solid lines are guides to the eye. Note that the logarithmic scale is used for vertical axis in (i) and (j).

performed high energy resolution inelastic neutron scattering experiments. Figure 5 shows the magnetic field dependence of the magnetic excitation spectra at the magnetic zone center measured at 3.5 K. As shown in Figs. 5(a) and 5(f), multiple excitation peaks are observed at zero magnetic field. This behavior is consistent with that reported in Ref. [23], in which the excitations were found to originate from a Zeeman ladder [24–29].

With the increase of the magnetic field, the peaks are shifted gradually. The magnetic field dependence of the lowest energy mode is summarized in Fig. 6. The lowest energy mode at (0, 0, 2), which is a degenerate transverse mode (S_X and S_Y) at zero magnetic field, is considered to split in magnetic field, as shown in Figs. 5(a)–5(e). The lower energy mode gradually decreases and finally goes below 0.4 meV at 8 T, where static S_Z order is destroyed. This indicates that the low energy mode in Fig. 4(e) is almost gapless. On the other hand, the higher energy mode gradually increases and the intensity gradually decreases with increase field. The higher energy modes at zero magnetic field also shift and may split in magnetic field. However, it is difficult to discuss the detailed field dependence from our data.

The scattering intensity at (0, 3, 1), shown in Figs. 5(f)–5(j), originates from 100%, 20%, and 80% of S_X, S_Y, and S_Z components, respectively, as that at (0, 6, 2). Therefore, at (0, 3, 1) a transverse mode (S_X) and the longitudinal mode (S_Z) are mostly observed. There are two excitation peaks at

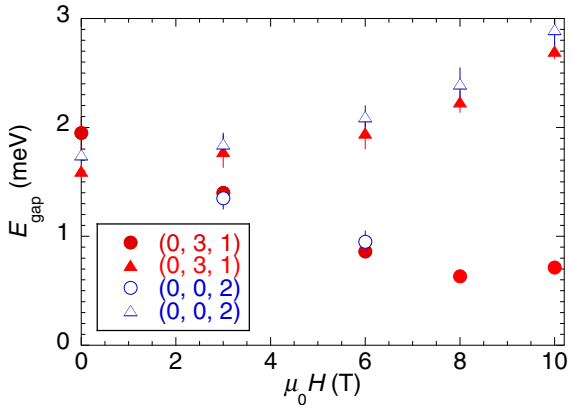

FIG. 6. Magnetic excitation gap energies at the magnetic zone center measured at 3.5 K as a function of magnetic field, obtained from the magnetic excitation spectra shown in Fig. 5. Only the split peaks of the lowest energy mode is plotted. The filled and open symbols represent the data points observed at (0, 3, 1) and (0, 0, 2), respectively.

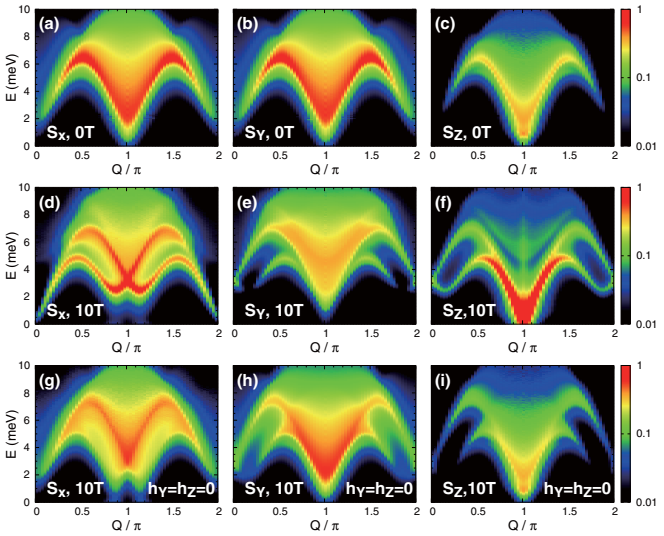

FIG. 7. $\tilde{S}(Q,E)$ calculated by the DMRG method using the spin Hamiltonian [Eq. (2)]. (a)–(c) and (d)–(f) are for 0 and 10 T, respectively. (g)–(i) are for 10 T with no staggered field ($h_Y = h_Z = 0$).

1.6 and 1.95 meV at zero magnetic field. It was identified that the former and later peaks correspond to transverse (S_X) and longitudinal (S_Z) modes, respectively [23]. The longitudinal mode is more intense and softens gradually with increasing magnetic field. Above 8 T, the excitation becomes much intense and shifts to higher energy with increasing magnetic field. Since there is no such low-energy peak at (0, 0, 2) above 8 T, where S_X and S_Y are observed, this mode is considered to come from S_Z. This is consistent with the assignment of the 1.95 meV peak as S_Z mode [23]. The transverse (S_X) mode, which is less intense, shifts to higher energy gradually. This behavior is similar to that of the higher energy mode at (0, 0, 2). The intensity at (0, 0, 2) is stronger because of larger magnetic form factor at lower Q. These results indicate that the lower energy mode at (0, 0, 2) originates from S_Y, which show similar magnetic field dependence as S_Z, observed at (0, 3, 1), up to 6 T. The S_Y mode becomes almost gapless above 8 T. The magnetic field dependence of the low energy excitation modes is consistent with that observed by electron spin resonance (ESR) measurements [30], considering that the critical magnetic field (∼10 T) in the ESR study is higher because the measurements were performed at a lower temperature (1.5 K). In our study, we identified the spin component relevant to each mode.

The low energy features of the magnetic excitations in a magnetic field are consistent with those shown in Fig. 4. At 10 T, incommensurate magnetic modes are observed at ∼2 meV around (0, 0, 2). On the other hand, the low-energy mode around (0, 6, 2), where the gap is small, is very intense. As described above, the incommensurate excitations with the band minimum at ∼2 meV, shown in Fig. 4(e), and the intense excitation, shown in Fig. 4(f), originate from S_X and S_Z mode, respectively. These experimentally observed features are reasonably well reproduced by the theoretical calculation based on the $S = \frac{1}{2}$ XXZ AF chain model, as shown in Figs. 4(i) and 4(j). Detailed discussion will be given in the next subsection.

2. *Theoretical results*

In Fig. 7 we show $\tilde{S}(Q,E)^{\alpha\alpha}$ calculated using the spin Hamiltonian of Eq. (2) with the parameters in Ref. [8]. To clarify relevant spin components in magnetic excitations, the intensities for S_X, S_Y, and S_Z are separately shown. At 0 T, S_X and S_Y represent the transverse mode and S_Z represents the longitudinal mode. The intensity mainly lies near the lower edge of a spinon band, indicating a spinon dispersion. The spinon dispersion has minima at $Q = 0$ and π, while the spin gap opens there because of the Ising-like anisotropy. Note that the total integrated intensity of S_Z is weak compared with those of S_X and S_Y because the zero-energy Lorentzian peak at $Q = \pi$ is subtracted for S_Z, while there is no such subtraction for S_X and S_Y.

With applying magnetic field, the spinon dispersion splits, as shown for 10 T in Figs. 7(d)–7(f). At first glance, the magnetic field dependence is quite different on each spin component. For S_X, two dispersive modes crossing at the zone center $Q = \pi$ are clearly visible due to a relatively large spectral weight along them compared with excitation continuum. The momentum position of the dispersion minimum shifts away from the zone center, leading to incommensurate gapped minima. Note that incommensurate gapless modes appear in the Heisenberg chain under magnetic field [12–15]. In the Heisenberg case, the incommensurate soft mode moves from $Q = \pi$ to 0 in the longitudinal component, and from $Q = 0$ to π in the transverse ones. In the present Ising-like case, the incommensurate mode is gapped. The incommensurate position moving from $Q = \pi$ toward 0 agrees with the longitudinal component. On the other hand, the energy position, where the two incommensurate modes cross at the zone center, gradually shifts toward high energy. The energy integrated intensity at the zone center is reduced. These observations are consistent with the experimental result, shown by triangles in Fig. 6. In contrast, for S_Y and S_Z, the splitting of the magnetic excitation mode is not observed at the zone center, but more distinct

around the zone boundary $Q = 0$. In fact, both S_Y and S_Z have incommensurate gapped minima near the zone boundary. The shift of the incommensurate position from $Q = 0$ to π agrees with the transverse component. Furthermore, the characteristic feature is that a gap mode at the zone center in S_Z is very intense, which is consistent with the experimental result. The peak is at 0.5 meV, which is slightly lower energy than the experimentally observed peak at around 0.7 meV. Note here that the zero-energy Lorentzian peaks at $Q = 0$ and π are subtracted for S_X and S_Y, respectively.

To clarify a key role of the effective staggered magnetic field, DMRG calculations were also performed without the staggered field, by setting $h_Y = h_Z = 0$ and keeping the other parameters unchanged. Results are presented in Figs. 7(g)–7(i). The overall structure of each component looks similar to that with the staggered field. However, the distribution of the spectral weight is rather different comparing the calculated spectra with and without the staggered field. For S_X, two incommensurate modes are observed, whereas a high-energy edge has large intensity rather than a low-energy edge. This is in contrast to the case with the staggered field, where the two modes are equally weighted. The change of the intensity distribution is also found for S_Y and S_Z. In particular, the intensity around a small gap mode at the zone center in S_Z is much reduced. Thus, a large dynamic magnetic structure factor in S_Z originates from the staggered field. Here the Lorentzian peaks at $Q = 0$ and π are subtracted for S_X and S_Z, respectively. Note that, irrespective of with and without the staggered field, the static magnetic structure at 10 T is "up-down-up-down" type. Only the difference is the spin direction, i.e., the Y and Z directions for with and without the staggered field, respectively. Therefore, the X direction is perpendicular to the AF moment in both cases and S_X is expected to show similar excitations. This suggests that the effect of the staggered field does not cause a significant change of the dispersion itself, but affects the intensity distribution, so that the incommensurate excitations become more visible.

As described in Sec. IV B 1, experimental data involve a mixture of three spin components. In order to compare the experimental and theoretical results in a more direct way, appropriate fractions of the three components are summed up, as shown in Figs. 4(g)–4(j). At 0 T, since there is no remarkable difference among the spectral shapes of the three components, the excitation spectrum looks similar regardless of fractions of the three components. At 10 T, the calculated intensity in Fig. 4(i) is in good agreement with the incommensurate correlations observed around (0, 0, 2) experimentally [Fig. 4(e)]. The theoretical result does not explain the gaplesslike mode observed around (0, 0, 2) which is intense. This is probably because the critical magnetic field is estimated to be ∼6 T with the parameters in Ref. [8], so that the gap energy at 10 T is calculated to be much higher than the observed value. On the other hand, Fig. 4(j) reasonably reproduces the observed excitations around (0, 6, 2) with regard to the intense peak at the zone center, originating from the S_Z mode [Fig. 4(f)]. The theoretical results shows the crossing structure at the zone center, originating from the S_X mode, whereas it is missing in the experimental results probably due to a small magnetic form factor. As shown in Fig. 5(j), the intensity at 2.8 meV is much weaker than that at 0.7 meV.

V. SUMMARY

We performed elastic and inelastic neutron scattering experiments in $BaCo_2V_2O_8$, consisting of fictitious $\frac{1}{2}$ spins of the Co^{2+} ions with Ising-like anisotropy, in a magnetic field perpendicular to the chain direction. The AF order of S_Z in zero magnetic field is completely suppressed by 8 T of magnetic field along the a axis at 3.5 K. Most importantly, we found that the AF order of S_Y gradually develops with increasing magnetic field along the a axis. This is the direct experimental evidence which shows the induced magnetic moments due to the staggered field perpendicular to the external magnetic field. We also studied magnetic excitations as a function of transverse magnetic field. The lower boundary of the spinon excitations splits gradually with increasing magnetic field. The overall feature of the magnetic excitation spectra in a magnetic field is reproduced by the theoretical calculation based on the $S = \frac{1}{2}$ 1D XXZ AF model, in which a large dynamic magnetic structure factor of S_Z and distinct incommensurate correlations of S_X are predicted.

ACKNOWLEDGMENTS

The research at ORNL's HFIR was sponsored by the Scientific User Facilities Division, Office of Basic Energy Sciences, US Department of Energy. Work at NIST was supported in part by the National Science Foundation under Agreement No. DMR-0944772. This study was supported in part by the U.S.-Japan Cooperative Program on Neutron Scattering. The authors were supported by JSPS and MEXT KAKENHI Grants No. JP16K05494, No. JP15K05192, No. JP16H01082, No. JP24244059, No. JP25246006, and No. JP25220803. Computations were done on the supercomputers at the Japan Atomic Energy Agency and the Institute for Solid State Physics, the University of Tokyo.

This manuscript has been authored by UT-Battelle, LLC under Contract No. DE-AC05-00OR22725 with the U.S. Department of Energy. The United States Government retains and the publisher, by accepting the article for publication, acknowledges that the United States Government retains a nonexclusive, paid-up, irrevocable, world-wide license to publish or reproduce the published form of this manuscript, or allow others to do so, for United States Government purposes. The Department of Energy will provide public access to these results of federally sponsored research in accordance with the DOE Public Access Plan (http://energy.gov/downloads/doepublic-access-plan).

[1] I. Affleck, J. Phys.: Condens. Matter **1**, 3047 (1989).
[2] F. D. M. Haldane, Phys. Rev. Lett. **45**, 1358 (1980).
[3] A. Luther and I. Paschel, Phys. Rev. B **12**, 3908 (1975).

[4] S. Kimura, H. Yashiro, K. Okunishi, M. Hagiwara, Z. He, K. Kindo, T. Taniyama, and M. Itoh, Phys. Rev. Lett. **99**, 087602 (2007).
[5] S. Kimura, T. Takeuchi, K. Okunishi, M. Hagiwara, Z. He, K. Kindo, T. Taniyama, and M. Itoh, Phys. Rev. Lett. **100**, 057202 (2008).
[6] S. Kimura, M. Matsuda, T. Masuda, S. Hondo, K. Kaneko, N. Metoki, M. Hagiwara, T. Takeuchi, K. Okunishi, Z. He, K. Kindo, T. Taniyama, and M. Itoh, Phys. Rev. Lett. **101**, 207201 (2008).
[7] Y. Kawasaki, J. L. Gavilano, L. Keller, J. Schefer, N. Christensen, A. Amato, T. Ohno, Y. Kishimoto, Z. He, Y. Ueda, and M. Itoh, Phys. Rev. B **83**, 064421 (2011).
[8] S. Kimura, K. Okunishi, M. Hagiwara, K. Kindo, Z. He, T. Taniyama, M. Itoh, K. Koyama, and K. Watanabe, J. Phys. Soc. Jpn. **82**, 033706 (2013).
[9] E. Canévet, B. Grenier, M. Klanjšek, C. Berthier, M. Horvatić, V. Simonet, and P. Lejay, Phys. Rev. B **87**, 054408 (2013).
[10] S. K. Niesen, G. Kolland, M. Seher, O. Breunig, M. Valldor, M. Braden, B. Grenier, and T. Lorenz, Phys. Rev. B **87**, 224413 (2013).
[11] D. V. Dmitriev, V. Ya. Krivnov, and A. A. Ovchinnikov, Phys. Rev. B **65**, 172409 (2002).
[12] E. Pytte, Phys. Rev. B **10**, 4637 (1974).
[13] N. Ishimura and H. Shiba, Prog. Theor. Phys. **64**, 479 (1980).
[14] G. Müller, H. Thomas, H. Beck, and J. C. Bonner, Phys. Rev. B **24**, 1429 (1981).
[15] J. C. Talstra and F. D. M. Haldane, Phys. Rev. B **50**, 6889 (1994).
[16] R. Coldea, D. A. Tennant, R. A. Cowley, D. F. McMorrow, B. Dorner, and Z. Tylczynski, Phys. Rev. Lett. **79**, 151 (1997).
[17] D. C. Dender, P. R. Hammar, D. H. Reich, C. Broholm, and G. Aeppli, Phys. Rev. Lett. **79**, 1750 (1997).
[18] M. B. Stone, D. H. Reich, C. Broholm, K. Lefmann, C. Rischel, C. P. Landee, and M. M. Turnbull, Phys. Rev. Lett. **91**, 037205 (2003).
[19] J. R. D. Copley and J. C. Cook, Chem. Phys. **292**, 477 (2003).
[20] R. T. Azuah, L. R. Kneller, Y. Qiu, P. L. W. Tregenna-Piggott, C. M. Brown, J. R. D. Copley, and R. M. Dimeo, J. Res. Natl. Inst. Stand. Technol. **114**, 341 (2009).
[21] S. R. White, Phys. Rev. Lett. **69**, 2863 (1992).
[22] E. Jeckelmann, Phys. Rev. B **66**, 045114 (2002).
[23] B. Grenier, S. Petit, V. Simonet, E. Canévet, L.-P. Regnault, S. Raymond, B. Canals, C. Berthier, and P. Lejay, Phys. Rev. Lett. **114**, 017201 (2015); **115**, 119902(E) (2015).
[24] H. Shiba, Prog. Theor. Phys. **64**, 466 (1980).
[25] N. Ishimura and H. Shiba, Prog. Theor. Phys. **63**, 743 (1980).
[26] S. E. Nagler, W. J. L. Buyers, R. L. Armstrong, and B. Briat, Phys. Rev. B **27**, 1784 (1983).
[27] R. Coldea, D. A. Tennant, E. M. Wheeler, E. Wawrzynska, D. Prabhakaran, M. Telling, K. Habicht, P. Smeibidl, and K. Kiefer, Science **327**, 177 (2010).
[28] C. M. Morris, R. Valdés Aguilar, A. Ghosh, S. M. Koohpayeh, J. Krizan, R. J. Cava, O. Tchernyshyov, T. M. McQueen, and N. P. Armitage, Phys. Rev. Lett. **112**, 137403 (2014).
[29] Z. Wang, M. Schmidt, A. K. Bera, A. T. M. N. Islam, B. Lake, A. Loidl, and J. Deisenhofer, Phys. Rev. B **91**, 140404(R) (2015).
[30] A. Okutani, S. Kimura, T. Takeuchi, and M. Hagiwara, Appl. Magn. Reson. **46**, 1003 (2015).